9120 *Inorg. Chem.* **2009**, *48*, 9120–9132
DOI: 10.1021/ic9004642

Inorganic Chemistry
Article

Mixed-Ligand Copper(II) Maltolate Complexes: Synthesis, Characterization, DNA Binding and Cleavage, and Cytotoxicity

Archika Barve,[†] Avinash Kumbhar,*[,†] Menakshi Bhat,[‡] Bimba Joshi,[‡] Ray Butcher,[§] Uddhavesh Sonawane,[⊥] and Rajendra Joshi[⊥]

[†]*Department of Chemistry and* [‡]*Institute of Bioinformatics and Biotechnology, University of Pune, Pune 411007, India,* [§]*Chemistry Department, Howard University, Washington, D.C. 20059, and* [⊥]*Bioinformatics Team, Centre for Development of Advanced Computing (C-DAC), Pune 411007, India*

Received March 9, 2009

The mixed-ligand complexes [Cu(L)(maltol)] where L = 2,2′-bipyridine (bpy; **1**), 1,10-phenanthroline (phen; **2**), 1,10-phenanthroline-5,6-dione (phendione; **3**), dipyrido[3,2-*a*:2′,3′-*c*]phenazine (dppz; **4**), and 4b,5,7,7a-tetrahydro-4b,7a-epiminomethanoimino-6*H*-imidazo[4,5-*f*][1,10]-phenanthroline-6,13-dione (bipyridylglycoluril; bpg; **5**) have been synthesized and characterized by structural, analytical, and spectral methods. The single-crystal X-ray structures of **1**, **2**, and **5** exhibit a distorted square-pyramidal structure, with the polypyridyl ligands and maltol occupying equatorial positions and either a water or nitrate anion at the axial position. The *N*,*N*-dimethylformamide glass as well as the single-crystal electron paramagnetic resonance of the complexes confirms the distorted square-pyramidal structure. The DNA binding investigated using different techniques (absorption titration, viscosity, thermal melting, and fluorescence quenching) indicates the partial intercalation of the planar polypyridyl ligands into DNA. The complexes cleave plasmid pBR322 DNA by a hydrolytic mechanism. The kinetic aspects of DNA cleavage under pseudo-Michaelis−Menten and true Michaelis−Menten conditions as well as the phosphodiesterase activity using model 4-nitrophenylphosphate are also detailed. The cytotoxicity of the complexes against HeLa (cervical) cancer cell lines shows that synergy between the metal and ligands results in a significant enhancement in the cell death with IC_{50} of ∼150−270 μg mL^{-1}.

Introduction

A precise understanding of the DNA binding properties of transition-metal complexes is of paramount importance because of their potential use as drugs, regulators of gene expression, and tools for molecular biology and nanotechnology.[1−5] The clinical success of cisplatin[6−9] and related platinum-based drugs, as anticancer agents that bind covalently to DNA, is severely affected by the serious side effects, general toxicity, and acquired drug resistance. This is an impetus to inorganic chemists to develop innovative strategies for the preparation of more effective, less toxic, target-specific, and preferably noncovalently bound anticancer drugs.[10,11] Transition-metal poplypyridyl complexes have been at the forefront of these investigations because of their unusual electronic properties, diverse chemical reactivity, and peculiar structure, which result in noncovalent interactions with DNA.[12] Sigman and co-workers have developed the first chemical nuclease $[Cu(phen)_2]^+$ that effectively cleaves B-DNA in the minor groove in the presence of a reducing agent[13−15] and also exhibits antiviral activity, which

*To whom correspondence should be addressed. E-mail: askum@chem.unipune.ernet.in. Tel: (+91)-020-25601397 (ext. 534). Fax: (+91)-020-25691728.

(1) Pyle, A. M.; Barton, J. K.; Lippard, S. J. *Prog. Inorg. Chem.* **1990**, *38*, 413.
(2) Burrows, C. J.; Rokita, S. E. *Acc. Chem. Res.* **1994**, *27*, 295.
(3) Tullius, T. D. *Metal−DNA Chemistry*; ACS Symposium Series 402; American Chemical Society: Washington, DC, 1989.
(4) Balaraman, S.; Venugopal, R.; Maheshwari, P. U.; Evans, H. S.; Palaniandavar, M. *J. Inorg. Biochem.* **2006**, *100*, 316.
(5) Banerjee, A. R.; Jaeger, A.; Turner, D. H. *Biochemistry* **1993**, *32*, 153.
(6) Boulikas, T.; Vougiouka, M. *Oncol. Rep.* **2003**, *10*, 1663.
(7) Wong, E.; Giandomenico, C. M. *Chem. Rev.* **1999**, *99*, 2451.
(8) Galanski, M.; Arion, V. B.; Jakupec, M. A.; Keppler, B. K. *Curr. Pharm. Des.* **2003**, *9*, 2078.
(9) Jamieson, E. R.; Lippard, S. J. *Chem. Rev.* **1999**, *99*, 2467.
(10) Tanaka, T.; Yukawa, K.; Umesaki, N. *Oncol. Rep.* **2005**, *14*, 1365.
(11) (a) Wang, D.; Lippard, S. J. *Nat. Rev. Drug Discovery* **2005**, *4*, 307–320. (b) Berners Price, S. J.; Appleton, T. G. In *Platinum-Based Drugs in Cancer Therapy*; Kelland, L. R., Farrell, N., Eds.; Humana Press: Totowa, NJ, 2000; pp 3−31. (c) Angeles-Boza, A. M.; Bradley, P. M.; Fu, P. K.-L.; Wicke, S. E.; Bacsa, J.; Dunbar, K. M.; Turro, C. *Inorg. Chem.* **2004**, *43*, 8510.
(12) (a) Metcalfe, C.; Thomas, J. A. *Chem. Soc. Rev.* **2003**, *32*, 215. (b) Erkkila, K. E.; Odom, D. T.; Barton, J. K. *Chem. Rev.* **1999**, *99*, 2777.
(13) Sigman, D. S.; Mazumder, A.; Perrin, D. M. *Chem. Rev.* **1993**, *93*, 2295.
(14) (a) Pope, L. E.; Sigman, D. S. *Proc. Natl. Acad. Sci. U.S.A.* **1984**, *81*, 3. (b) Sigman, D. S. *Biochemistry* **1990**, *29*, 9097. (c) Kuwara, M. D.; Sigman, D. S. *Biochemistry* **1987**, *26*, 7234. (d) Mazumder, M.; Chen, C. B.; Gaynor, R. P.; Sigman, D. S. *Nucleic Acids Res.* **1994**, *22*, 2255.
(15) Ren, R.; Yang, P.; Zheng, W.; Hua, Z. *Inorg. Chem.* **2000**, *39*, 5454.

 Published on Web 08/27/2009

inhibits proviral DNA synthesis.[16] A number of mononuclear copper(II) polypyridyl and mixed-ligand polypyridyl complexes, viz., $[Cu(dpq)_2(H_2O)]^{2+}$,[17] $[Cu(dppz)_2Cl]^{+}$,[18] $[Cu(L)Cl_2]^{2+}$ (where L = 5,5′-diguanidylmethyl-2,2′-bipyridyl cation[19] and 5,5′-di-1-aminomethyl-2,2′-bipyridyl cation),[20] and $[Cu(imda)L]$[21] (where imda = iminodiacetic acid and L = 1, 10-phenanthroline, 5,6-dimethyl-1,10-phenanthroline, and dipyrido[3,2-*d*:2′,3′-*f*]quinoxaline), wherein the copper-bound hydroxyl is the active species that hydrolyzes the nucleic acid phosphate backbone have been reported. Recently, Reedjik and co-workers have reported efficient self-activated DNA cleavage and cytotoxic effects on L1210 murine leukemia and A 2780 human ovarian carcinoma cell lines by the complexes $[Cu(pyrimol)Cl]$[22] and $[Cu(pbt)Br_2]$[23] [pbt = 2-(2-pyridyl)benzthiazole]. The in vitro antitumor effect of $[Cu(phendione)_3]^{2+}$ on human epithelial cell lines has also been studied.[24] Mixed-ligand copper(II) phenolate complexes of the type $[Cu(tdp)L]^{+}$ (where tdp = 2-[(2-(2-hydroxyethylethylimino)methyl]phenol and L = diimine ligand) exhibit anticancer activity with potency greater than that of cisplatin and mitomycin against the human cervical epidermoidal carcinoma (ME180) cell line.[25] Other complexes, like copper(II) phenanthroline L-threonine[26] and copper(II) phenanthroline diisopropyl salicylato,[27] exhibit cytotoxicity and antiviral activity. Similarly, complexes of the types [Cu(phen)(edda)][28] and [Cu(phen)(*N*-propylnorfloxacin)Cl][29] exhibit anticancer and antileukemic activity, respectively, indicating that the synergy between the metal and ligand results in enhancement of their antiproliferative properties. The dimeric copper complex of an unsymmetric ligand *N*-(2-hydroxybenzyl)-*N*,*N*′,*N*′-tris(2-pyridylmethyl)-1,3-diaminopropan-2-ol (H_2btppnol) promotes hydrolysis of the P−O phosphate diester bond, hydrolytically cleaves plasmid DNA at physiological pH, and is cytotoxic to a human carcinoma cell line.[29b]

Therefore, in the present work, we report the synthesis, structural characterization, nuclease activity, phosphodiesterase activity, and cytotoxicity of [Cu(L)(maltol)] (where maltol is 3-hydroxy-2-methyl-4-pyrone and L is polypyridyl ligands), as shown in Scheme 1. The rationale for the choice of maltol as the coligand is that it serves as a chelator for many metal ions and its complexes with oxovanadium(IV) and iron(III) are reported to be insulin enhancers with a potential use in the treatment of diabetes,[30−34] and it was also used as an oral drug to remove the excess of iron in thallasaemia or hemochromatosis.[35] Maltolate anion is a good leaving group in DNA-targeted complexes.[36] Maltol-mediated stimulation of transition-metal reduction with concomitant generation of reactive oxygen species causing apoptosis-inducing, antimicrobial, and antitumoral effects is also documented.[37,38] Thus, in the present series of complexes, we have an ensemble of polypyridyl ligands with varying intercalating ability, a bioavailable redox metal ion, copper, a prooxidant coligand, maltol, and coordinated aqua/nitrate ligands, which can act as nucleophiles toward phosphodiester bonds in nucleic acids.

Experimental Section

Reagents and Materials. All reagents and solvents were purchased commercially and were used as received. $Cu(NO_3)_2\cdot 3H_2O$, 2,2′-bipyridine, and 1,10-phenanthroline were obtained from SRL (India), and maltol was obtained from Lancaster (U.K.). Calf thymus DNA (CT-DNA) was purchased from SRL (India). The enzyme superoxide dismutase (SOD EC1.15.1.1) was purchased from Sigma Chemical Co. Deionized water was used for preparation of the buffers. Supercoiled pBR322 DNA (CsCl purified) was obtained from Bangalore Genei (Bangalore, India) and used as received.

Synthesis of Polypyridyl Ligands. The ligands 1,10-phenenthroline-5,6-dione (phendione)[39] and dipyrido[3,2-*a*:2′,3′-*c*]phenazine (dppz)[40] were synthesized according to literature protocols. 4b,5,7,7a-Tetrahydro-4b,7a-epiminomethanoimino-6*H*-imidazo[4,5-*f*][1,10]phenanthroline-6,13-dione (bpg) was prepared by modification of the literature methods.[41,42]

Synthesis of Complexes. [Cu(bpy)(maltol)(NO_3)] (1). An aqueous solution of $Cu(NO_3)_2\cdot 3H_2O$ (1 mmol) was added to a solution of 2,2′-bipyridine (1 mmol) and maltol (1 mmol) in

(16) Morrow, J. R.; Trogler, W. C. *Inorg. Chem.* **1988**, *27*, 3387.
(17) Dhar, S.; Reddy, P. A. N.; Chakravarty, A. R. *Dalton Trans.* **2004**, 697.
(18) Gupta, T.; Dhar, S.; Nethaji, M.; Chakravarty, A. R. *Dalton Trans.* **2004**, 1896.
(19) Yan, A.; Tong, M. L.; Ji, L.-N.; Mao, Z. W. *Dalton Trans.* **2006**, 2066.
(20) Juan, H.; Ping, H.; Wang, Y.; Tong, M.; Sun, H.; Mao, Z.; Ji, L.-N. *Dalton Trans.* **2008**, 3207.
(21) (a) Selvakumar, B.; Rajendiran, V.; Maheshwari, P. U.; Stoeckli-Evans, H.; Palaniandavar, M. *J. Inorg. Biochem.* **2006**, *100*, 316. (b) Dhar, S.; Nethaji, M.; Chakravarty, A. R. *Inorg. Chem.* **2005**, *44*, 8876. (c) Patra, A. K.; Nethaji, M.; Chakravarty, A. R. *Dalton Trans.* **2005**, 2798.
(22) Maheshwari, P. U.; Roy, S.; Dulk, H. D.; Barendes, S.; Wezel, G. V.; Kozlevkar, B.; Gamez, P.; Reedjik, J. *J. Am. Chem. Soc.* **2006**, *128*, 710.
(23) Maheshwari, U. P.; Ster, M. V. D.; Smulders, S.; Barendes, S.; Wezel, G. P. V.; Massera, C.; Roy, S.; Dulk, H. D.; Gamez, P.; Reedjik, J. *Inorg. Chem.* **2008**, *47*, 3719.
(24) Deegan, C.; Coyle, B.; McCann, M.; Devereux, M.; Egan, D. A. *Chem.−Biol. Interactions* **2006**, *164*, 115.
(25) Rajendiran, V.; Karthik, S.; Palaniandavar, M.; Stoeckli-Evans, H.; Periasamy, V. S.; Akbarsha, M. A.; Srirang, B. S.; Krishnamurthy, H. *Inorg. Chem.* **2007**, *46*, 8208.
(26) Zhang, S.; Zhu, Y.; Tu, C.; Wei, H.; Yang, Z.; Lin, L.; Ding, J. *J. Inorg. Biochem.* **2004**, *98*, 2099.
(27) Ranford, J. D.; Sadler, P. J.; Tocher, D. A. *J. Chem. Soc., Dalton Trans.* **1993**, *22*, 3393.
(28) Ng, C. H.; Kong, K. C.; Von, S. T.; Balraj, P.; Jensen, P.; Thirthagiri, E.; Hamada, H.; Chikira, M. *Dalton Trans.* **2008**, 447.
(29) (a) Katsarou, M.; Efthimiadou, E.; Psomas, G.; Karliota, A.; Vourloumis, D. *J. Med. Chem.* **2008**, *51*, 470. (b) Rossi, L. M.; Neves, A.; Bortoluzzi, A. J.; Horner, R.; Szpoganicz, B.; Terenzi, H.; Mangrich, A. S.; Pereira-Maia, E.; Castellano, E. E.; Hasse, W. *Inorg. Chim. Acta* **2005**, *358*, 1807. (c) Neves, A.; Rossi, L. M.; Horn, A., Jr.; Vencato, I.; Bortoluzzi, A. J.; Zucco, C.; Mangrich, A. S. *Inorg. Chem. Commun.* **1999**, *2*, 334.
(30) Thompson, K. H.; McNeill, J. H.; Orvig, C. *Chem. Rev.* **1999**, *99*, 2561.
(31) Rehder, D.; Pessoa, J. C.; Geraldes, C. F. G. C.; Castro, M. M. C. A.; Kabanos, T.; Kiss, T.; Meier, B.; Micera, G.; Petterson, L.; Rangel, M.; Salifoglou, A.; Turel, I.; Wang, D. *J. Biol. Inorg. Chem.* **2002**, *7*, 384.
(32) Crans, D. C.; Mahroof-Tahir, M.; Johnson, M. D.; Wilkins, P. C.; Yang, L.; Robbins, K.; Johnson, A.; Alfano, J. A.; Godzala, M. E., III; Austin, L. T.; Willsky, G. R. *Inorg. Chim. Acta* **2003**, *356*, 365.
(33) Sakurai, H.; Fujisawa, Y.; Fujimoto, S.; Yasui, H.; Takino, T. *J. Trace Elem. Exptl. Med.* **1999**, *12*, 393.
(34) Krosniak, M.; Zachwieja, B.; Zygmunt, M.; Grybos, Z. R. *Arch. Pharm. Pharm. Med. Chem.* **2001**, *334*, 338.
(35) Ahmed, S. I.; Burgess, J.; Fawcett, J.; Parsons, S. A.; Russell, D. R.; Laurie, S. H. *Polyhedron* **2000**, *19*, 129.
(36) Carland, M.; Tan, K. J.; White, J. M.; Stephenson, J.; Murray, V.; Denny, W. A.; McFadyen, W. D. *J. Inorg. Biochem.* **2005**, *99*, 1738.
(37) Murakami, K.; Ishida, K.; Watakabe, K.; Tsubouchi, R.; Naruse, M.; Yoshino, M. *Toxicol. Lett.* **2006**, *161*, 102.
(38) Murakami, K.; Ishida, K.; Watakabe, K.; Tsubouchi, R.; Haneda, M.; Yoshino, M. *Biometals* **2006**, *19*, 253.
(39) Yamada, M.; Tanaka, Y.; Yoshimoto, Y.; Kuroda, S. *Bull. Chem. Soc. Jpn.* **1992**, *65*, 1006.
(40) Dickerson, J. E.; Summers, L. A. *Aust. J. Chem.* **1970**, *23*, 1023.
(41) Elemans, J. A. A. W.; Gelder, R. D.; Rowan, A. E.; Nolte, R. J. M. *Chem. Commun.* **1998**, 1553.
(42) Kurth, D. G.; Fromm, K. M.; Lehn, J. M. *Eur. J. Inorg. Chem.* **2001**, 1523.

Scheme 1. Structures of Polypyridyl Ligands and Maltol Used in the Present Study

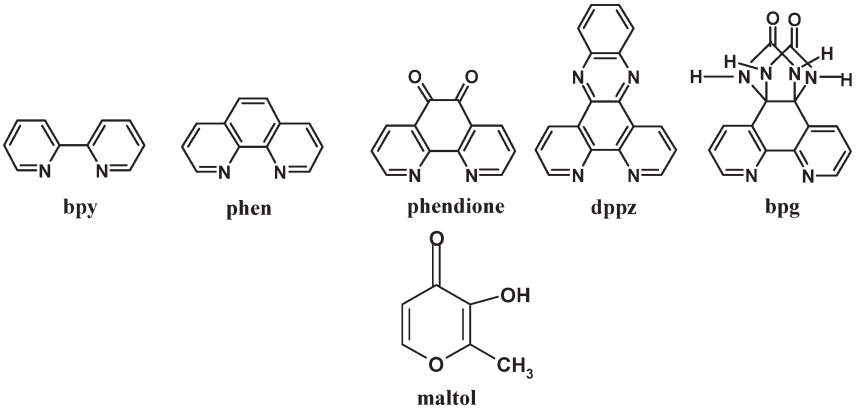

30 mL of methanol and was refluxed for 3 h. After 2−3 days, green crystals suitable for X-ray analysis were collected (yield: 78%). Other complexes are prepared similarly by using appropriate polypyridyl ligands. Elem anal. Found (calcd) for $C_{16}H_{13}N_3O_6Cu$: C, 46.93 (47.23); H, 3.18 (3.22); N, 10.15 (10.32). UV−vis (H_2O, nm) (ε, M^{-1} cm^{-1}): 646 (35). FT-IR (ν, cm^{-1}): 549, 613, 1031, 1280, 1388,1654. μ_{eff} (300 K): 1.68 μ_B. Λ_m (S m^2 M^{-1}) in water at 27 °C: 237.

[Cu(phen)(maltol)(H_2O)](NO_3)·H_2O (2). The complex was prepared using a procedure similar to that for **1** by using 1,10-phenanthroline instead of 2,2′-bipyridine. Elem anal. Found (calcd) for $C_{18}H_{17}N_3O_8Cu$: C, 46.25 (46.30); H, 3.50 (3.56); N, 8.96 (9.00). UV−vis (H_2O, nm) (ε, M^{-1} cm^{-1}): 650 (42). FT-IR (ν, cm^{-1}): 549, 609, 1039, 1276, 1396, 1651, 1562, 3350. μ_{eff} (300 K): 1.70 μ_B. Λ_m (S m^2 M^{-1}) in water at 27 °C: 243.

[Cu(phendione)(maltol)(H_2O)](NO_3)·H_2O (3). The complex was prepared using a procedure similar to that for **1** by using 1,10-phenanthroline-5,6-dione instead of 2,2′-bipyridine. Elem anal. Found (calcd) for $C_{18}H_{17}N_3O_{11}Cu$: C, 41.96 (41.99); H, 3.30 (3.32); N, 8.13 (8.15). UV−vis (H_2O, nm) (ε, M^{-1} cm^{-1}) 649, 548 (43). FT-IR (ν, cm^{-1}): 501, 630, 1066, 1278, 1384, 1645, 1616, 1579, 1579, 3360, 1716. μ_{eff} (300 K): 1.61 μ_B. Λ_m (S m^2 M^{-1}) in water at 27 °C: 251.

[Cu(dppz)(maltol)(H_2O)](NO_3)·$2H_2O$ (4). The complex was prepared using a procedure similar to that for **1** by using dipyrido[3,2-*a*:2′,3′-*c*]phenazine instead of 2,2′-bipyridine. Elem anal. Found (calcd) for $C_{24}H_{21}N_5O_9Cu$: C, 49.05 (49.10); H, 3.52 (3.60); N, 11.6 (11.93). UV−vis (H_2O, nm) (ε, M^{-1} cm^{-1}): 580, 456, 377 (40, 316). FT-IR (ν, cm^{-1}): 580, 615, 1043, 1230, 1388, 1614, 1530, 3375. μ_{eff} (300 K): 1.70 μ_B. Λ_m (S m^2 M^{-1}) in water at 27 °C: 235.

[Cu(bpg)(maltol)(NO_3)]·$0.3H_2O$ (5). The complex was prepared using a procedure similar to that for **1** by using 4b,5,7,7a-tetrahydro-4b,7a-epiminomethanoimino-6*H*-imidazo[4,5-*f*]-[1,10]-phenanthroline-6,13-dione instead of 2,2′-bipyridine. Elem anal. Found (calcd) for $C_{20}H_{21}N_7O_{11}Cu$: C, 39.94 (40.17); H, 3.20 (3.53); N, 16.30 (16.38). UV−vis (H_2O, nm) (ε, M^{-1} cm^{-1}): 643 (38). FT-IR (ν, cm^{-1}): 550, 612, 1033, 1284, 1389, 1565, 1556. μ_{eff} (300 K): 1.63 μ_B. Λ_m (S m^2 M^{-1}) in water at 27 °C: 240.

Methods and Instrumentation. FT-IR spectra were recorded as KBr pellets on a Perkin-Elmer FT-IR 283-B spectrophotometer at the Microanalytical Laboratory, University of Pune. Electronic absorption spectra were recorded on a Shimadzu UV−vis spectrophotometer (UV 1601) in the range of 250−900 nm using a matched pair of 1 cm quartz cells at University of Pune. Electrochemical studies were performed in a dimethyl sulfoxide (DMSO) solvent on a Bioanalytical System BAS CV-27 and a CH Instruments model 1100A with an *X*− *Y* recorder in our laboratory using a three-compartment cell consisting of a 2 mm diameter platinum inlay working electrode, a platinum wire as an auxiliary electrode, and a saturated calomel electrode (SCE) as a reference electrode. Tetraethylammonium perchlorate (TEAP; 0.1 M) was used as a supporting electrolyte. ^1H NMR spectra of ligands were measured on a Varian-Mercury 300 MHz spectrometer with $CDCl_3$ and DMSO-d_6 as solvents at room temperature. All chemical shifts are given relative to tetramethylsilane as the internal standard. Magnetic susceptibilities at room temperature were measured on a Faraday balance calibrated using mercury(II) tetrathiocyanatocobalt(II) as a calibrant. Molar conductivity measurements were made using an Equiptronics model EQ 664 conductivity meter. The electron spin resonance (ESR) spectra were recorded in DMSO at 77 K on a Varian X-Band spectrophotometer at Regional Sophisticated Instrument Center, Indian Institute of Technology, Powai, Mumbai, India, using tetracyanoethylene as the internal standard. Single-crystal ESR spectra were recorded after a 10° rotation at one axis.

Single-Crystal X-ray Diffraction Studies. Single-crystal X-ray structures of the complexes **1**, **2**, and **5** were collected on a Bruker three-circle platform diffractometer equipped with a SMART 1000 CCD detector. All data were corrected for Lorentzian, polarization, and absorption effects. The program package *SHELX-97*[43] (Sheldrick, G. M. *SHELX-97 program for crystal structure solution and refinement*; University of Göttingen: Göttingen, Germany, 1997) was used for structure solution and full matrix least-squares refinement on F^2. Hydrogen atoms for the cations were included in the refinement as per the riding model. Hydrogen atoms for some of the water molecules were obtained by a difference map and were refined by keeping the isotropic thermal parameters fixed.

DNA Binding Experiments. CT-DNA was used for binding studies with the various copper(II) mixed-ligand polypyridyl complexes investigated during this work. The stock solution was prepared by dissolving CT-DNA in a phosphate buffer (pH 7.2) and kept overnight at 4 °C for complete dissolution. The DNA concentration per nucleotide was determined by absorption spectroscopy using the molar absorption coefficient (6600 M^{-1} cm^{-1}) at 260 nm. Solutions of CT-DNA in a phosphate buffer gave a ratio of absorbance at 260 and 280 nm of 1.8−1.9:1, indicating that the DNA was sufficiently free of protein.[44]

Competitive Binding Fluorescence Measurements. Emission intensity measurements were carried out using a Shimadzu spectrofluorimeter. A phosphate buffer was used as a blank to make preliminary adjustments. The extinction wavelength was fixed, and the emission range was adjusted before measurements. DNA was pretreated with ethidium bromide (EBR) in the ratio [NP]:[EBR] = 1:1 for 15 min. The metal complexes

(43) Sheldrick, G. M. *SHELX-97 Program for Crystal Structure Refinement*; University of Göttingen: Göttingen, Germany, 1997.
(44) Marmur, J. *J. Mol. Biol.* **1961**, *3*, 208.

were then added to this mixture, and their effect on the emission intensity was measured.[45]

Viscosity Measurements. Viscosity experiments were carried out using a semimicroviscometer maintained at 28 °C in a thermostatic water bath. The flow time of solutions in a phosphate buffer (pH 7.2) was recorded in triplicate for each sample, and an average flow time was calculated. Data were presented as $(\eta/\eta_0)^{1/3}$ versus the binding ratio, where η is the viscosity of DNA in the presence of a complex and η_0 is the viscosity of DNA alone. Viscosity values were calculated from the observed flow time of DNA-containing solutions (t) corrected for that of buffer alone (t^0), $\eta = t - t^0$.[46,47]

DNA Thermal Denaturation Studies. Thermal melting curves were obtained on a Jasco UV−vis spectrophotometer with a Peltier assembly (ETC 717) connected to a temperature controller. The melting curves were recorded at the same molar ratio of the compound to DNA (r) by measurements of the changes in absorption at 260 nm as function of the temperature in the range 25−95 °C. T_m values were determined from the maximum of the first derivative or tangentially from the graph at the midpoint of the transition curves. ΔT_m values were calculated by subtracting T_m of the free nucleic acid from T_m of the nucleic acid interacted with the complex.[48]

DNA Cleavage Experiments. DNA Cleavage Studies Using Agarose Gel Electrophoresis. Electrophoresis through agarose is the standard method used to separate, identify, or purify DNA fragments. When an electric field is applied across the gel, DNA, which is negatively charged at neutral pH, migrates toward the anode. The intact supercoiled (SC, form I) DNA migrates faster than the single-nicked (NC, form II) DNA in the gel. This technique has been employed to identify the products of DNA cleavage, which was carried out in this work.

A 10 μL total sample volume in 0.5 mL transparent eppendorf microtubes contains pBR322 DNA (100 ng) and a metal complex. For the gel electrophoresis experiments, supercoiled pBR322 DNA was treated with the metal complex and the mixture was incubated for 30 min at 37 °C. The samples were analyzed by 1% agarose gel electrophoresis [Tris−boric acid−ethylenediaminetetraacetic acid (EDTA) (TBE) buffer, pH 8.2] for 3 h at 60 mV. The gel was stained with 0.5 μg mL^{-1} ethidium bromide, visualized by UV light, and photographed for analysis. The extent of cleavage of the SC DNA was determined by measuring the intensities of the bands using the Alpha Innotech Gel Documentation System (AlphaImager 2200). For mechanistic investigations, experiments were carried out in the presence of radical scavenging agents, viz., DMSO, mannitol, DABCO ($OH^\bullet$ radical), NaN_3, L-histidine ($^1O_2$ radical), and SOD ($O^{\bullet 2-}$ radical), which were added to SC DNA prior to the addition of the complex.

Kinetic Measurements Using the Gel Electrophoresis Technique. For kinetic measurements, DNA cleavage rates at various complex concentrations were measured in a TBE buffer (pH 8.2) at 37 °C for different intervals of time. After incubation and irradiation of the DNA and copper(II) complexes for a defined time, 2 μL of the loading buffer (0.25% bromophenol blue, 0.25% xylene cyanol, 40% glycerol, and 2 mM EDTA) was added. The samples were then loaded directly onto a 1% agarose gel and electrophoresed at a constant voltage of 60 mV. The gels were viewed in an Alpha Innotech Gel Documentation System and photographed using a digital camera, and densitometric calculations were performed using the software provided by Alpha Innotech. The decrease in the intensities of form I were then plotted against complex concentrations, and these were fitted well with a single-exponential decay curve (pseudo-first-order kinetics) by use of eq 1, where y_0 is the initial percentage of a form of DNA, y is the specific form of DNA at time t, const is the percentage of uncleaved DNA, K_{obs} is the hydrolysis rate or apparent rate constant, and V_{max} is the maximal reaction velocity. Careful optimization of electrophoretic and densitometric techniques led to pseudo-first-order kinetics and allowed the determination of true Michaelis−Menten kinetic parameters.

$$y = (y_0 - \text{const}) \exp(-K_{obs} x) + \text{const} \quad (1)$$

K_{obs}' versus [Cu] was plotted and fit using eq 2, which allows the determination of both the rate constants and Michaelis−Menten-"type" kinetic values. Similar experiments with constant complex concentrations and varying DNA (10−90 μM) concentrations were performed, and the intensities were plotted against substrate concentrations by use of eq 3.

$$K_{obs}' = V_{max}'[\text{catalyst}]/(K_M + [\text{catalyst}]) \quad (2)$$

$$K_{obs} = V_{max}[\text{substrate}]/(K_M + [\text{substrate}]) \quad (3)$$

T4 Ligase Enzymatic Assay. DNA ligation is used in order to link DNA fragments end-to-end using either complementary overhangs, "sticky" ends, or "blunt" ends. The enzyme used to catalyze the ligation reaction was T4 DNA ligase from *Escherichia coli* phage T4. This enzyme covalently links the DNA strands by generating a phosphodiester bond between 3′-hydroxy and 5′-phosphate groups. Low-melting agarose was used for T4 ligase gel electrophoresis experiments and were carried out at low temperature.

An enzymatic assay was performed using T4 DNA ligase to determine whether the cleaved products were consistent with hydrolysis of the phosphodiester linkages in DNA.[48] For the religation experiments, the NC DNA obtained from the hydrolytic cleavage reaction was recovered from agarose gel by the phenol extraction method and purified by ethanol precipitation. A mixture of 1 μL of 10× ligation buffer, 4 units of T4 DNA ligase, and NC DNA was incubated at 16 °C for 18 h prior to gel electrophoresis.

Kinetic Measurements Using 4-(Nitrophenyl)phosphate (NPP; Phosphodiesterase Activity). Hydrolysis of NPP produces 4-nitrophenolate with a maximum absorbance at 400 nm and an extinction coefficient of 18 700 mol^{-1} cm^{-1}. The initial rate of production of 4-nitrophenolate was monitored spectrophotometrically at 400 nm, and the concentration of 4-nitrophenolate produced was calculated from the extinction coefficient.

To correct the spontaneous hydrolysis of the phosphodiester, the rate of each reaction was measured against the reference cell, which was identical in composition but lacked the complex. The reaction was monitored up to 1 h until saturation. The initial rate of reaction was obtained directly from a plot of the 4-nitrophenolate concentration versus time, which was linear. Reactions were performed in a phosphate buffer, and an ionic strength of 0.10 M was maintained with $NaNO_3$.[49,50]

Cytotoxicity Studies. Cytotoxicity studies were carried out on a HeLa cell line, which was obtained from National Center for Cell Science, Pune University, Pune, India.

(a) Cell Viability Assay. Cell viability was carried out using the MTT assay method.[51] The cells were seeded in a 24-well plate

(45) Ramkrishnan, S.; Palaniandavar, M. *Dalton Trans.* **2008**, 3866.
(46) Cohen, G.; Eisenberg, H. *Biopolymers* **1969**, *8*, 45.
(47) Deshpande, M. S.; Kumbhar, A. A.; Kumbhar, A. S.; Kumbhakar, M.; Pal, H.; Sonawane, U. B.; Joshi, R. R. *Bioconjugate Chem.* **2009**, *20*, 447.
(48) He, J.; Hu, P.; Wang, Y.-J.; Tong, M.-L.; Sun, H.; Mao, Z.-W.; Ji, L.-N. *Dalton Trans.* **2008**, 3207.
(49) (a) Pamatong, F. V.; Detmer, A. C., III; Bocarsly, J. R. *J. Am. Chem. Soc.* **1996**, *118*, 5339. (b) Sreedhara, A.; Freed, J. D.; Cowan, J. A. *J. Am. Chem. Soc.* **2000**, *122*, 8814.
(50) Deck, K. M.; Tseng, T. A.; Burstyn, J. N. *Inorg. Chem.* **2002**, *41*, 669.
(51) Blagosklonny, M.; EI-diery, W. S. *Int. J. Cancer* **1996**, *67*, 386.
(52) (a) Meyer, B. N.; Ferrigni, N. R.; Putnam, J. E.; Jacobsen, L. B.; Nichols, D. E.; McLaughlin, L. L. *Planta Med.* **1982**, *45*, 31. (b) Latha, L. Y.; Sasidharan, S.; Zuraini, Z.; Suryani, S.; Shirley, L.; Sangetha, S.; Davaselvi, M. *Afr. J. Tradit., Complementary, Altern. Med.* **2007**, *4*, 59.

at a density of 104 cells well^{-1} in Dulbuco's Modified Eagle's Medium containing 10% fetal calf serum and a 0.1% antibiotic solution for 24 h at 37 °C and 5% CO_2 for adherence. Complexes **1**−**5**, in a concentration of 50−400 μg mL^{-1}, dissolved in DMSO and distilled water, were added to the wells with a fresh medium. DMSO was used as a vehicle control. After every 24, 48, and 72 h of incubation, MTT assay was carried out. A MTT solution (20 μL, 5 mg mL^{-1}) prepared in a 10 mM phosphate buffer was added to each well and incubated for 4 h. The purple formazan product was dissolved by addition of 100 μL of 100% DMSO for 5 min. The absorbance was measured at 570 and 630 nm using an ELISA plate reader, and the viability was calculated. Data were collected for three replicates each and were used to calculate the mean. The percentage inhibition was calculated from this data:

$$\%\ \text{inhibition} = \frac{\text{mean OD of untreated cells (control)}}{\text{mean OD of treated cells (control)}} \times 100$$

(b) Brine Shrimp Method. The toxicity test of complexes **1**−**5** was carried out on brine shrimp, *Artemia salina*, by the method of Meyer et al.[52a] Brine shrimp eggs were hatched in artificial seawater prepared from 20% commercial sea salt (Sigma Aldrich). After 48 h of incubation (at 25−29 °C), nauplii (larvae) were collected in a 96-well microtiter plate. Larvae (10−15) were added to each well containing a serially diluted complex (**1**−**5**; 50−480 μg dissolved in a DMF−water medium). After 24 h of incubation, live and dead larvae were counted and LC_{50} was determined for each plant extract, as shown by Latha et al.[52b]

Molecular Modeling. Molecular modeling studies were performed on a Silicon Graphics Octane workstation using the software *Insight II 2000*[53] with Discover 3 module at C-DAC, Pune, India. The initial models of right-handed B-DNA of sequence d(C:G)12 were constructed using the Biopolymer module of Insight II. The coordinates for the metal complex and derivatives were taken from its crystal structure as a CIF file and were converted to the PDB format using *Mercury* software.[54] The all-atom extensible systematic force field was used for the entire modeling study. The copper(II) complexes and derivative-bound DNA was then soaked in a water box of dimensions 35.0 × 50.0 × 35.0, and periodic boundary conditions were applied. A dielectric constant of 1.0 for the electrostatic energy and a cutoff of 9.5 Å were used for both the coulomb as well as van der Waals energies. The nonbonded electrostatic terms were calculated using the Ewald summation method. The accuracy of convergence for the Ewald coulomb energy summation was kept at 0.0001 kcal mol^{-1}. The system was minimized using the steepest-descent gradient algorithm for 1000 steps, followed by the conjugate gradient algorithm for 1000 steps or until the maximum derivative was below 0.1 kcal mol^{-1} Å^{-1}.

Results and Discussion

Syntheses and Structures of Mixed-Ligand Complexes. The mixed-ligand complexes [Cu(L)(maltol)], where L = bpy (**1**), phen (**2**), phendione (**3**), dppz (**4**), and bpg (**5**), have been isolated from the aqueous methanolic solution containing copper(II) nitrate as the starting material. All of the complexes were obtained in good yield and are characterized by using elemental analysis, UV−vis, IR, electron paramagnetic resonance (EPR) spectral studies,

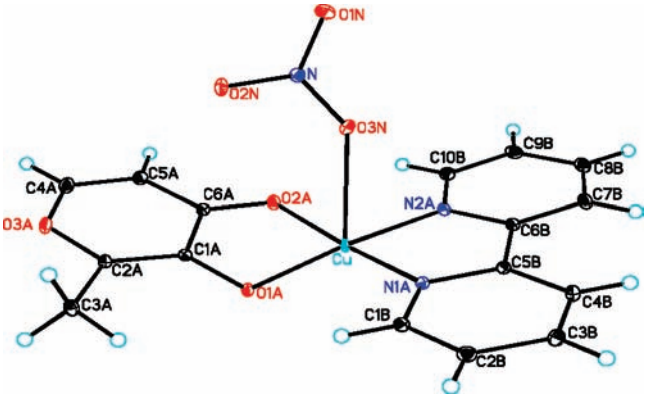

Figure 1. ORTEP diagram of complex **1** showing the atom numbering scheme. Thermal ellipsoids are drawn at 50% probability.

Table 1. Crystal Data and Structure Refinement for **1**

empirical formula	$C_{16}H_{13}CuN_3O_6$
fw	406.83
temperature (K)	103(2)
wavelength (Å)	0.7103
cryst syst	triclinic
space group	*P*1
unit cell dimens	*a* = 8.4403(10) Å, α = 84.046(2)°
	b = 8.8985(11) Å, *β* = 87.073(2)°
	c = 10.5639(13) Å, *γ* = 89.110(2)°
volume (Å^3)	788.06(17)
Z	2
density (calcd) (mg m^{-3})	1.714
abs coeff (mm^{-1})	1.428
F(000)	414
cryst size (mm^3)	0.40 × 0.45 × 0.64
θ range for data collection (deg)	1.94−28.40
index ranges	$-9 \le h \le 10, -10 \le k \le 11, -13 \le l \le 14$
reflns collected	5882
indep reflns	3677 [*R*(int) = 0.0409]
completeness of *θ* = 28.40° (%)	92.9
abs correction	semiempirical from equivalents
max and min transmn	0.894 387 and 0.781 582
refinement method	full-matrix least squares on F^2
data/restraints/param	3577/0/236
GOF on F^2	1.063
final *R* indices [$I > 2\sigma(I)$]	R1 = 0.0284, wR2 = 0.0763
R indices (all data)	R1 = 0.0304, wR2 = 0.0773
largest diff peak and hole (e Å^{-3})	0.471 and −0.548

and cyclic voltammetry. The room temperature magnetic moment of the complexes are in the range of 1.60−1.70 μ_B, indicating discrete mononuclear complexes, while molar conductivities are indicative of a 1:1 salt type, confirming the geometry. X-ray crystal structures of complexes **1**, **2**, and **5** have been determined. All complexes are soluble in water and a phosphate buffer (pH 7.2) except complex **5**, which is soluble in 10% DMF.

Crystal Structures of Complexes 1, 2, and 5. Crystal Structure of Complex 1 (CCDC Number 673676). The structure of complex **1** (Figure 1) consists of two discrete monomeric copper(II) species in the unit cell of the crystal system belonging to the space group *P*1 with the metal in a 4 + 1 square-pyramidal CuN_2O_3 coordination geometry in which the axial site has been occupied by a coordinated

(53) Insight II 2000. *Molecular Modelling Program Package*; Accelrys Inc.: San Diego, 1997.

(54) Mercury, Cambridge Crystallographic Data Centre, 12 Union Road, Cambridge CB21EZ, United Kingdom. Available from website: http://www.ccdc.cam.ac.uk/.

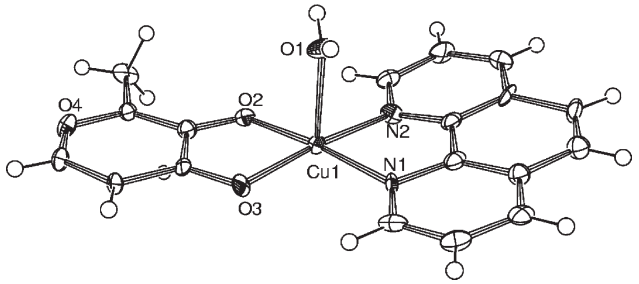

Figure 2. ORTEP diagram of complex **2** showing the atom numbering scheme. Thermal ellipsoids are drawn at 50% probability.

Table 2. Bond Lengths (Å) and Angles (deg) for Complex **1**

bond length		bond angle	
Cu−O1A	1.9360(11)	O1A−Cu−N2A	174.95(5)
Cu−O2A	1.9917(15)	O1A−Cu−O2A	84.46(5)
Cu−N2A	1.9928(12)	N2A−Cu−O2A	97.99(5)
Cu−N2B	1.9958(14)	O1A−Cu−N1A	93.18(5)
		N2A−Cu−N1A	81.74(5)
		O2A−Cu−N1A	174.57(5)
		O1A−Cu−O3N	85.01
		O3−N−Cu	2.514

Table 3. Crystal Data and Structure Refinement for **2**

empirical formula	$C_{36}\,H_{30}\,Cu_2\,N_6\,O_{14}$
fw	897.74
temperature (K)	293(2)
wavelength (Å)	0.710 69
cryst syst	triclinic
space group	*P*1
unit cell dimens	*a* = 7.683(5) Å, α = 99.205(5)°
	b = 10.436(5) Å, *β* = 102.283(5)°
	c = 12.205(5) Å, *γ* = 106.072(5)°
volume (Å^3)	893.5(8)
Z	1
density (calcd) (mg m^{-3})	1.668
abs coeff (mm^{-1})	1.272
F(000)	458
cryst size (mm^3)	0.1 × 0.1 × 0.2
θ range for data collection (deg)	2.39−28.29
index ranges	$-10 \le h \le 8$, $-13 \le k \le 13$, $-16 \le l \le 15$
reflns collected	5992
indep reflns	4994 [*R*(int) = 0.0118]
completeness of *θ* = 28.29° (%)	95.7
abs correction	none
refinement method	full-matrix least squares on F^2
absolute structure param	0.088(18)
data/restraints/param	4994/11/504
GOF on F^2	1.055
final *R* indices [$I > 2\sigma(I)$]	R1 = 0.0324, wR2 = 0.0890
R indices (all data)	R1 = 0.0346, wR2 = 0.0909
largest diff peak and hole (e Å^{-3})	0.659 and −0.705

nitrate molecule. The donor atoms in each basal plane are two nitrogen atoms from the polypyridyl ligand and two ortho oxygen atoms of the maltol ligand. The axial site has a coordinated nitrate molecule with a Cu−O distance of 2.514 Å compared to the equatorial Cu−O

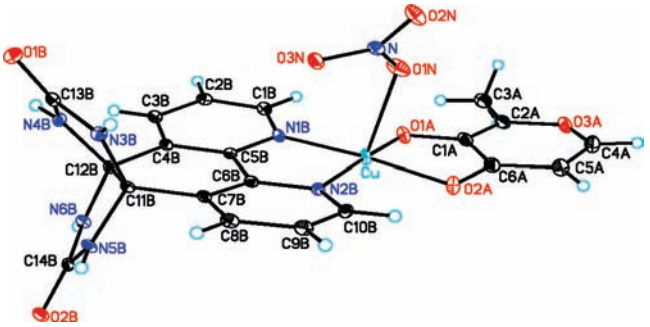

Figure 3. ORTEP diagram of complex **5** showing the atom numbering scheme. Thermal ellipsoids are drawn at 50% probability.

Table 4. Bond Lengths (Å) and Angles (deg) for Complex **2**

bond length		bond angle	
Cu1−O2	1.961(7)	O2−Cu1−N1	174.1(3)
Cu1−N1	1.979(7)	O2−Cu1−O3	84.7(3)
Cu1−O3	1.985(6)	N1−Cu1−O3	93.7(3)
Cu1−N2	1.996(7)	O2−Cu1−N2	97.8(3)
Cu1−O1	2.180(6)	N1−Cu1−N2	83.3(3)
Cu2−O6	1.905(6)	O3−Cu1−N2	174.9(3)
Cu2−O7	1.958(6)	O2−Cu1−O1	97.1(3)
Cu2−N3	2.024(7)	N1−Cu1−O1	88.6(3)
Cu2−N4	2.016(7)	O3−Cu1−O1	94.1(2)
Cu2−O5	2.183(6)	N2−Cu1−O1	90.0(3)
Cu1−Cu2	3.566	O6−Cu2−O7	85.9(3)
		O6−Cu2−N4	172.6(3)
		O7−Cu2−N4	95.7(3)
		O6−Cu2−N3	95.8(3)
		O7−Cu2−N3	174.7(3)
		N4−Cu2−N3	82.0(3)
		O6−Cu2−O5	97.4(3)
		O7−Cu2−O5	94.2(3)
		N4−Cu2−O5	89.7(3)
		N3−Cu2−O5	90.5(2)
		C13−O3−Cu1	108.1(5)

(approximately 1.93−1.99 Å), which is a consequence of tetragonal distortion, caused by the Jahn−Teller effect (one electron in the $d_{x^2-y^2}$ orbital). Figure S1 in the Supporting Information shows a packing diagram of complex **1** with hydrogen-bonding interactions between one of the oxygen atoms of the bound nitrate of one molecule and a hydrogen atom of the bipyridyl ligand of another molecule. The structure refinement parameters and crystal data for complex **1** are given in Table 1, and specific bond distances (Å) and bond angles (deg) are listed in Table 2.

Crystal Structure of Complex 2 (CCDC Number 673677). The structure of complex **2** consists of two discrete monomeric copper(II) species in the unit cell of the triclinic crystal system belonging to the space group *P*1 with the metal in a 4 + 1 square-pyramidal CuN_2O_3 coordination geometry and one lattice nitrate anion. The donor atoms in each basal plane are two nitrogen atoms from the heterocyclic base and the oxygen atoms of the maltol ligand. The axial site has a coordinated water molecule. The axial Cu−O (2.180 Å) distances are longer than the equatorial ones (approximately 1.96−1.99 Å), which is a consequence of tetragonal distortion caused by the Jahn−Teller effect. The packing diagram of complex **2** shows hydrogen-bonding interactions and the presence of nitrate molecules in the lattice (Figure 2). A weak

interaction between Cu1 and Cu2 is also observed, but the distance between the two copper centers is 3.566 Å. The structure refinement parameters and crystal data for complex **2** are given in Table 3, and specific bond distances (Å) and bond angles (deg) are listed in Table 4.

Table 5. Crystal Data and Structure Refinement for **5**

empirical formula	$C_{20}\,H_{21}\,Cu\,N_7\,O_{11}$
fw	598.98
temperature (K)	103(2)
wavelength (Å)	0.710 73
cryst syst	monoclinic
space group	*P*2(1)*c*
unit cell dimens	*a* = 8.9725 (10) Å, α = 90°
	b = 20.306 (2)Å, *β* = 107.929(2)°
	c = 12.9424 Å, *γ* = 90°
volume (Å^3)	2243.6(4)
Z	4
density (calcd) (mg m^{-3})	1.773
abs coeff (mm^{-1})	1.055
F(000)	1228
cryst size (mm^3)	0.30 × 0.38 × 0.84
θ range for data collection (deg)	1.93−28.28
index ranges	$-11 \le h \le 10$, $-26 \le k \le 27$, $-17 \le l \le 15$
reflns collected	17 208
indep reflns	5471 [*R*(int) = 0.0571]
completeness of *θ* = 28.28° (%)	98.4
abs correction	semiempirical from equivalents
max and min transmn	0.894 387 and 0.537 817
refinement method	full-matrix least squares on F^2
data/restraints/param	5471/9/370
GOF on F^2	1.023
final *R* indices [$I > 2\sigma(I)$]	R1 = 0.0530, wR2 = 0.1400
R indices (all data)	R1 = 0.0709, wR2 = 0.1476
largest diff peak and hole (e Å^{-3})	1.029 and −1.093

Table 6. Bond Lengths (Å) and Angles (deg) for Complex **5**

bond length		bond angle	
Cu−O1A	1.919(3)	O1A−Cu−O2A	85.59(11)
Cu−O2A	1.969(2)	O1A−Cu−N2B	173.93(11)
Cu−N2B	1.984(3)	O2A−Cu−N2B	96.33(11)
Cu−N1B	1.989(3)	O1A−Cu−N1B	95.51(11)
O1A−C1A	1.349(4)	O2A−Cu−N1B	175.65(11)
O2A−C6A	1.281(4)	N2B−Cu−N1B	82.15(10)
O3A−C4A	1.320(5)	C1A−O1A−Cu	107.8(2)
O3A−C2A	1.388(4)	C6A−O2A−Cu	109.0(2)
O1B−C13B	1.229(4)	C4A−O3A−C2A	121.2(3)
O2B−C14B	1.245(4)	O3N−N−O1N	121.0(3)
O1−N−Cu	2.460	O3N−N−O2N	119.3(3)
		O1N−N−O2N	119.7(3)
		C1B−N1B−Cu	127.2(2)
		C5B−N1B−Cu	113.9(2)
		C10B−N2B−Cu	126.6(2)
		C6B−N2B−Cu	113.7(2)

Crystal Structure of Complex 5 (CCDC Number 673678). The structure of complex **5** consists of two discrete monomeric copper(II) species in the unit cell of the crystal system belonging to the space group *P*2(1)*c* with the metal in a 4 + 1 square-pyramidal CuN_2O_3 coordination geometry and three lattice water molecules. The donor atoms in each basal plane are two nitrogen atoms from the heterocyclic base and oxygen atoms of the maltol ligand. The axial site has a coordinated nitrate anion. A nitrate molecule (O1N−Cu = 2.460 Å) occupying the axial position has a longer Cu−O distance than the equatorial Cu−O (maltol) (approximately 1.91−1.98 Å), which is a consequence of the tetragonal distortion caused by the Jahn−Teller effect (one electron in $d_{x^2-y^2}$ orbital). The packing diagram of the complex shows lattice water molecules (Figure 3). The structure refinement parameters and crystal data for complex **5** are given in Table 5, and specific bond distances (Å) and bond angles (deg) are listed in Table 6.

UV−Vis and IR Spectroscopy. Complexes **1**−**5** exhibit only one broad d−d band in the visible region (580−650 nm) with very low absorptivities (Figure S4 in the Supporting Information and Table 7), revealing a slightly distorted square-based copper(II) coordination geometry, which is consistent with the X-ray crystal structures of **1**, **2** and **5** and the EPR data of the complexes discussed below.

The IR spectra show a decrease in the *ν*(C=N) frequency for the ligands upon complexation, indicating the involvement of nitrogen in the coordination of metal ions. The data were further supported by the *ν*(Cu−O) band, which appeared at ∼500−515 cm^{-1}. The spectra show characteristic bands of nitrates in the range of 1000−1400 cm^{-1} and a coordinated water molecule in the 3300−3400 cm^{-1} range.[21] The IR bands in the region 530−560 cm^{-1} are assigned to *ν*(Cu−N) coordination. The fingerprint region shows bands due to stretching vibrations of the aromatic groups.

ESR Spectra of Complexes. The ESR spectra of complexes **1**−**5** were recorded at 77 K in DMSO (Figures 4 and S5 in the Supporting Information and Table 7). They are characteristic of Cu^{2+} and exhibited resolved features with $g_\parallel > g_\perp > 2$ and *G* in the range of 4.42−5.16 for all complexes, confirming that square-based geometries of the complexes, as observed in the X-ray crystal structure of complexes **1**, **2**, and **5**, are retained in solution. A square-based CuN_4 is expected to show a $g_\parallel$ value around 2.20 and a $A_\parallel$ value of (180−200) × 10^{-4} cm^{-1}, and replacement of nitrogen by an oxygen atom is expected to increase the $g_\parallel$ value and decrease the $A_\parallel$ value.

Single-Crystal ESR Spectra of Complexes 1, 2, and 5. ESR spectra for single crystals were recorded by rotating

Table 7. Spectroscopic, ESR, and Cyclic Voltammetric Data for Complexes **1**−**5**

complex	*λ* (nm) (d−d)	*ε* (M^{-1} cm^{-1}	$g_\parallel$	$g_\perp$	$A_\parallel$	$E_{1/2}$ vs SCE
[Cu(bpy)(maltol)(NO_3)]	646	35	2.30	2.06	88	+0.20
[Cu(phen)(maltol)(H_2O)]$^+$	650	42	2.31	2.06	85	+0.16
[Cu(phendione)(maltol)]$^+$	649	43	2.35	2.07	145	+0.08
[Cu(dppz)(maltol)]$^+$	580	40	2.31	2.07	160	+0.02
[Cu(bpg)(maltol)(NO_3)]	643	38	2.32	2.07	152	+0.18

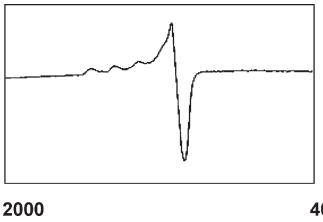

Figure 4. Liquid-nitrogen-temperature ESR spectra of complex **2** in DMSO.

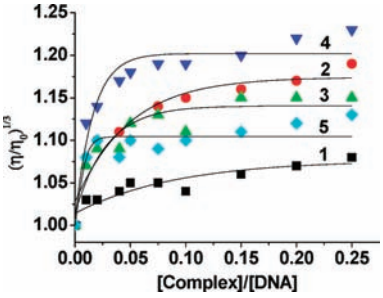

Figure 5. Change in the viscosity of CT-DNA (100 μM) in the presence of increasing amounts of copper complexes (1−100 μM) of **1**−**5**.

Table 8. Thermal Denaturation Studies of Complexes **1**−**5** with CT-DNA

complex	T_m (°C)	ΔT_m (°C)
DNA	67.96	
[Cu(bpy)(maltol)(NO_3)]	64.34	−3.59
[Cu(phen)(maltol)(H_2O)]$^+$	71.36	+3.4
[Cu(phendione)(maltol)]$^+$	68.05	+0.09
[Cu(dppz)(maltol)]$^+$	73.96	+6.0
[Cu(bpg)(maltol)(NO_3)]	68.94	+0.98

Table 9. Rate Constants for NPP Hydrolysis of Complexes **1**−**5**

complex	substrate	k(pH 7.2) (s^{-1})
CuLaL	NPP	1.20×10^{-2}
[Cu(oxpn)Ni(EDA)(H_2O)$_2$] (ClO_4)$_2$	NPP	7.80×10^{-4}
[Cu(oxpn)Ni(DMEDA)(H_2O)$_2$](ClO_4)$_2$	NPP	5.68×10^{-4}
[Cu(oxpn)Ni(DEEDA)(H_2O)$_2$] (ClO_4)$_2$	NPP	1.77×10^{-4}
[Cu(oxpn)Ni(DEPDA)(H_2O)$_2$] (ClO_4)$_2$	NPP	1.72×10^{-4}
1	NPP	2×10^{-3}
2	NPP	2.5×10^{-3}
3	NPP	0.75×10^{-3}
4	NPP	5×10^{-3}
5	NPP	4×10^{-3}

the crystal in one random plane. Although there are two molecules per unit cell, they are magnetically equivalent and thus showed a single line at 310−340° rotations in complex **1**, at 250, 260, 330, and 340° in complex **2**, and at 250−310° in complex **5**. Representative ESR spectra are shown in Figure S6 in the Supporting Information.

The spectra show one principal g value, g_3, parallel to the C_2 crystal axis. The spectra obtained by rotating around this direction gave the other two principal g values, g_1 and g_2. The g_1 direction, corresponding to the lowest g value, and g_2 are almost coincident with the

(55) (a) Bencini, A.; Gatteschi, D. *Inorg. Chem.* **1997**, *16*, 1994. (b) Subramanian, P. S.; Suresh, E.; Srinivas, D. *Inorg. Chem.* **2000**, *39*, 2053. (c) Hathway, B. J.; Billing, D. E.; Dubley, R. J.; Fereday, R. J.; Tomlinson, A. A. G. *J. Chem. Soc. A* **1970**, 806.

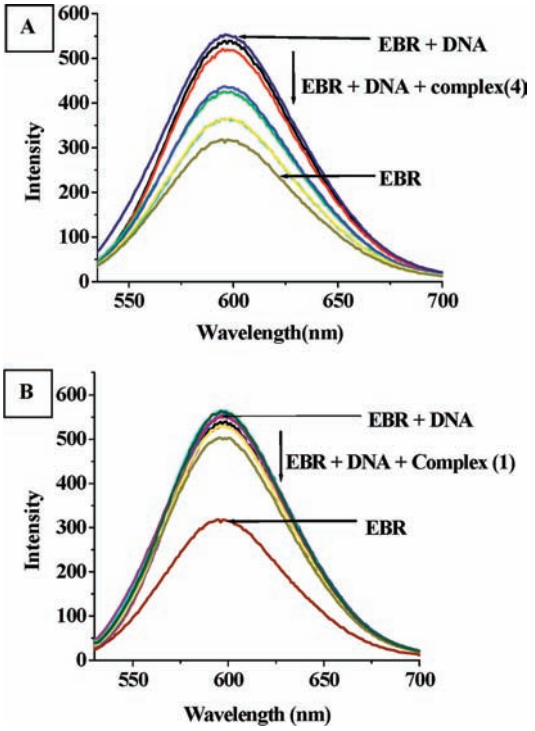

Figure 6. Fluorescence quenching curves of ethidium bromide bound to DNA: (A) complex **1**; (B) complex **4**. [DNA] = 20 μM, [EBR] = 20 μM, and [complex] = 0−200 μM.

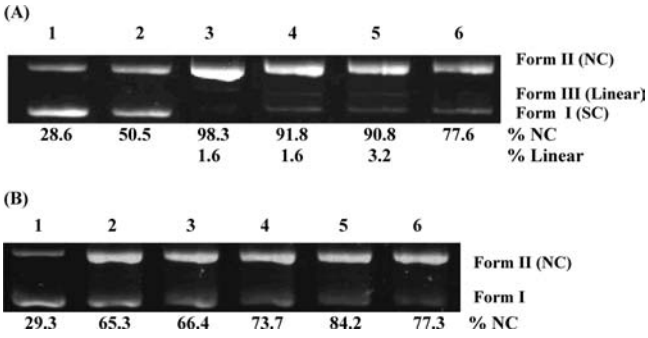

Figure 7. Ethidium bromide stained agarose gel (1%) of 100 ng μL^{-1} pBR322 plasmid DNA in the presence of 500 μM complex after 30 min of incubation (A) and under argon (B). Lane 1: DNA control. Lane 2: pBR322 + **1**. Lane 3: pBR322 + **2**. Lane 4: pBR322 + **3**. Lane 5: pBR322 + **4**. Lane 6: pBR322 + **5**.

projection of Cu−N2 and Cu−N2′. The g values of the present complexes (Table S7 in the Supporting Information) are similar to those of [Cu(phen)$_2$$H_2O$] ($NO_3$)$_2$[55] (2.02, 2.125, and 2.227) and [Cu(salEen)$_2$(ClO_4)$_2$][55a] and much different from those of [Cu(bpy)$_2$]I[55b] and better reflect the large anisotropy in the equatorial plane.

The value of g_3 in the Cu−O bond direction is larger than that in the Cu−I bond direction of [Cu(bpy)$_2$I] (2.66 vs 2.16), perhaps as a consequence of the different nephelauxetic properties of the two donors.

Electrochemical Studies. The electrochemical profiles of the ligand and complexes were studied in DMSO solvent by cyclic voltammetry in the range of +1 to −1 vs SCE using a platinum working electrode, a SCE reference electrode, and a platinum wire auxiliary electrode using TEAP as the supporting electrolyte. The copper complexes exhibit a reversible peak due to the Cu^{2+}/Cu^+

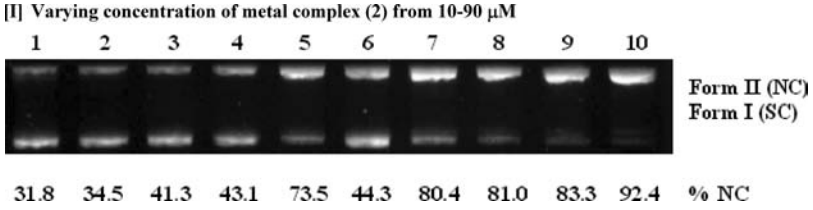

Figure 8. Saturation kinetics for the cleavage of plasmid DNA (100 ng μL^{-1}) by varying the complex concentration for 30 min at 37 °C in Tris-HCl/NaCl buffer (pH 8.0). Lane 1: DNA control. Lanes 2−10: DNA + [complex] = 10, 20, 30, 40, 50, 60, 70, 80, and 90 μM, respectively.

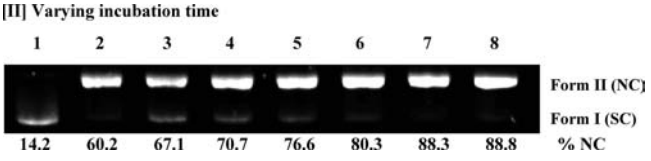

Figure 9. Kinetic analysis of the complex **2** DNA cleavage activity. Plasmid DNA (pBR 322, 100 ng μL^{-1}) and 100 μM complex **2** incubated at 370 °C for 0, 5, 10, 15, 20, 25, and 30 min, respectively. Lanes 2−8 and lane 1: DNA control.

redox couple, indicating the presence of an identical structural arrangement. The plot of ip_c and ip_a vs $\nu^{1/2}$ is a straight line, indicating a diffusion-controlled reaction. The positive range shows that a facile reduction of Cu^{2+} to Cu^{+} is possible, similar to other polypyridine complexes. The Cu^{II}/Cu^{I} redox potentials of all complexes (**1**−**5**) display significant variations depending upon the π-delocalized diimines in the order of **4** > **3** > **2** > **5** > **1**. However, the π delocalization of the electron density from copper into the extended planar ring of dppz destabilizes the Cu^{II} oxidation state.

DNA Binding Properties. Because DNA is the primary pharmacological target of many antitumor compounds, the interaction between DNA and metal complexes is of paramount importance in understanding the mechanism. Thus, the mode and propensity for binding of the complex to CT-DNA were studied with the aid of different techniques.

Viscosity Measurements. Viscosity measurements are sensitive to length changes of DNA and are regarded as the most critical test for the binding mode.[46,47] The effects of the complexes on the viscosities of DNA are shown in Figure 5. Under appropriate conditions, intercalation causes a significant increase in the viscosity of DNA solutions due to an increase in the separation of base pairs at the intercalation site, resulting in an increase in the overall DNA contour length. There is a small increase in the viscosity of DNA for almost all complexes compared to classical intercalator ethidium bromide.

EBR and the ability of the complexes to increase the viscosity of DNA follow the order **4** > **2** > **3** ~ **5** > **1**. The significant increase in the viscosity of complexes **2** and **4** indicates partial intercalative binding to DNA. The viscosity changes for complexes **1**, **3**, and **5** are negligible, indicating that the polypyridyl ligands in these complexes do not intercalate within the base pairs, as is expected because of their nonplanar nature.

Thermal Denaturation Studies. The interactions of all of the copper complexes with CT-DNA are characterized by measuring their effects on the melting temperature of DNA (Table 8). An increase in the melting temperature was observed in complexes **2** (+3.4) and **4** (6.0), indicative of the partial intercalation of phen and dppz ligands between the DNA base pairs causing stabilization of the base stack typical of partially intercalating metal complexes,[21,48] whereas in complexes **1**, **3**, and **5**, negligible or lower ΔT_m (°C) values are indicative of their nonintercalative DNA binding due to the loss of planarity of the polypyridyl ligands.

Fluorescence Spectroscopic Studies. The UV−visible spectra of the complexes are dominated by ligand transition bands and weak ligand-to-metal charge-transfer bands (λ = 400−520 nm; ε = 30−150 mol^{-1} cm^{-1}) and d−d transition bands at around 600−700 nm. The complexes, however, are nonfluorescent upon excitation in the visible region. The competitive binding of the copper(II) complexes with CT-DNA has been studied by a fluorescence spectral method. Measurements have been carried out using the emission intensity of ethidium bromide bound to DNA as a probe. Ethidium bromide is an intercalator that gives a significant emission when bound to DNA. Its displacement from DNA by a metal complex results in a decrease in the fluorescence intensity. In the competitive binding studies, the copper(II) complexes were added to CT-DNA pretreated with ethidium bromide and then the emission intensities of DNA-induced EBR were measured. The results are shown in Figures 6 and S8 in the Supporting Information, where it is seen that, with the addition of a copper complex to DNA, there is an appreciable decrease in the emission intensity. The extent of reduction of the emission intensity gives a measure of the binding propensity of the complex to DNA. Complex **4** is a strong binder to DNA than complexes **1**−**3** and **5**.

NPP Hydrolysis. More recently, progress has been made in the study of metal complexes that promote phosphodiester hydrolysis.[29b,56] All complexes catalyze the hydrolysis of NPP with an inflection observed between pH 8 and 9, indicating that under these experimental conditions only one metal-coordinated water molecule underwent acid association; thus, the active species in the hydrolysis reaction is the aquo−hydroxo form of the complex. The rate constants determined for complexes **1**−**5** shown in Table 9 are of the order of 10^{-3} s^{-1} and are similar to the other copper complexes showing hydrolysis of NPP.

DNA Cleavage Studies: Without Added Reductant. To assess the DNA cleavage ability of the complexes, supercoiled pBR322 DNA (100 ng μL^{-1}) was incubated with 500 μM of all complexes in 5 mM Tris-HCl/50 mM NaCl buffer at pH 8 (Figure 7) for 30 min without the addition of a reductant.[47,57] Control experiments show that all

(56) Rossi, L. M.; Neves, A.; Horner, R.; Terenzi, H.; Szpoganicz, B.; Sugai, J. *Inorg. Chim. Acta* **2002**, *337*, 366.
(57) (a) Tonde, S. S.; Kumbhar, A. S.; Padhye, S. B.; Butcher, R. J. *J. Inorg. Biochem.* **2006**, *100*, 51. (b) Ghosh, S.; Barve, A. C.; Kumbhar, A. A.; Kumbhar, A. S.; Puranik, V. G.; Datar, P. A.; Sonawane, U. B.; Joshi, R. R. *J. Inorg. Biochem.* **2006**, *100*, 331. (c) Deshpande, M. S.; Kumbhar, A. A.; Kumbhar, A. S. *Inorg. Chem.* **2007**, *46*, 5450.

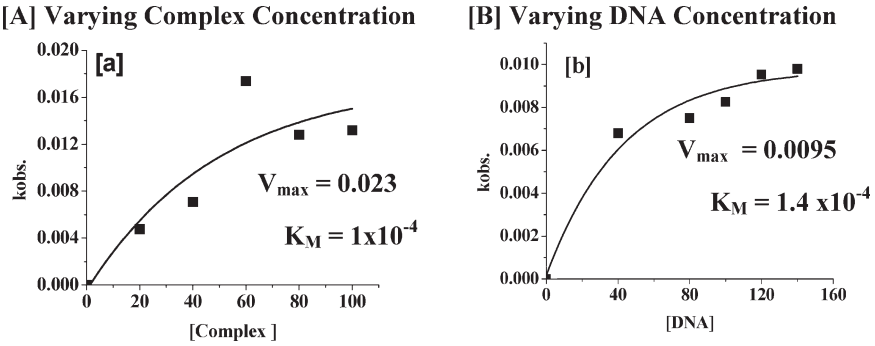

Figure 10. (A) Saturation kinetics of the cleavage of SC pBR322 DNA (100 ng μL^{-1}) using complex **2** with different concentrations of the complex (20−100 μM) in a Tris-HCl buffer (pH 8.0) followed at 37 °C. (B) Saturation kinetics of the cleavage of SC pBR322 DNA using 60 μM complex **2** with different concentrations of DNA (40−140 μM) in a Tris-HCl buffer (pH 8.0) followed at 37 °C.

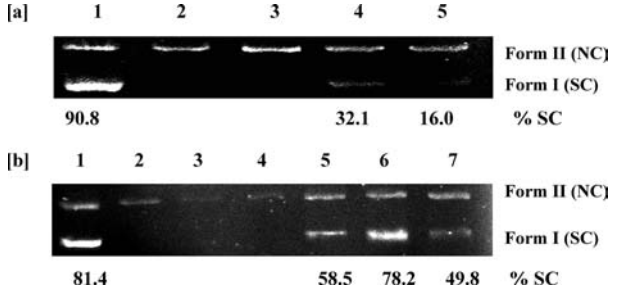

Figure 11. (a) Lane 1: DNA control. Lanes 2 and 3: products (nicked plasmid pBR322 of complexes **1** and **2**) obtained from reaction with the complex after an incubation period of 30 min. Lanes 4 and 5: complexes **1** and **2** + T4 ligase after 18 h of incubation. (b) Lane 1: DNA control. Lanes 2−4: products (nicked plasmid pBR322 of complexes **3**−**5**) obtained from reaction with the complex after an incubation period of 30 min. Lanes 5−7: complexes **3**−**5** + T4 ligase after 18 h of incubation. Lanes 4 and 5: lanes 2−4 + T4 ligase.

ligands and $Cu(NO_3)_2$ are cleavage inactive. The SC DNA (form I) was cleaved by all complexes, and the percentage of form II thus formed was ~95% in the case of complexes **2**−**4** and approximately 80% in complex **5**. The formation of form III linear DNA, observed in the case of complexes **2**−**4**, indicated a hydrolytic cleavage mechanism supported by the fact that DNA cleavage occurs under an argon atmosphere for all of the complexes. Such DNA hydrolysis by copper(II), which contains the Lewis acid (Cu^{II}) center, an avid DNA groove binder (phen, phendione, bpy, and bpg) and a bound aqua/nitrate ligand suitable for intramolecular nucleophilic activation have been reported earlier.[17−21]

Investigation of the DNA Cleavage Mechanism in the Presence of Radical Scavengers. The involvement of reactive oxygen species (hydroxyl, superoxide, singlet oxygen, and hydrogen peroxide) in the nuclease mechanism can be inferred by monitoring of the quenching of the DNA cleavage in the presence of radical scavengers in solution. Complexes **1**−**5** do not show inhibition of DNA cleavage in the presence of scavengers of hydroxyl radicals (DMSO, mannitol, and DABCO), singlet oxygen (sodium azide and L-histidine), and superoxide radical scavengers (SOD). This indicates that the cleavage of DNA probably follows a hydrolytic cleavage mechanism (Figure S9 in the Supporting Information).

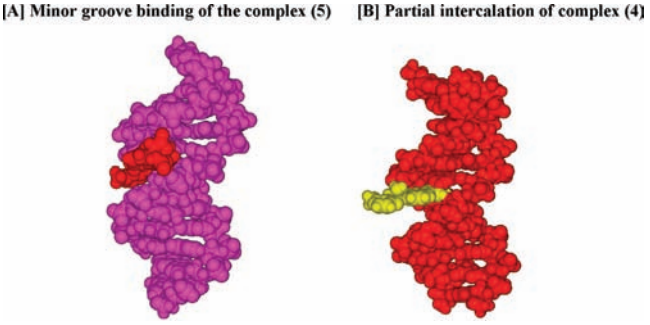

Figure 12. (A) Space-filling models of complex **5** bound to DNA in the minor groove. (B) Space-filling model of complex **4** showing partial intercalation.

Distamycin Assay. The groove selectivity of the complexes was determined from the control experiments using minor groove binder distamycin A.[58] Significant inhibition of the DNA cleavage activity of complexes **1**−**3** and **5** has been observed in the presence of distamycin A bound SC DNA, indicating the minor groove binding nature of the complexes, while no inhibition in cleavage was observed in the presence of complex **4** (Figure S10 in the Supporting Information), which indicates a major groove binding of complex **4** similar to that of $[Cu(dppz)_2Cl]^+$.[18] On the basis of all of these results, we propose that compound **4** interacts with DNA through the major groove and compounds **1**−**3** and **5** interact through the minor groove of DNA.

Kinetics of 2 in the Presence of Plasmid pBR322 DNA. Reactions were carried out under pseudo-Michaelis−Menten conditions by using various concentrations of **2** from 10 to 90 μM and a constant DNA concentration (100 ng μL^{-1}), which resulted in the formation of form II, as shown in Figure 8. Also, the DNA cleavage was studied by variation of the incubation time shown in Figure 9. The increase in form II fitted well to a single-exponential decay curve and followed pseudo-first-order kinetics (Figure 10A). The rates of cleavage were calculated to give the kinetic parameters $V_{max}' = 0.023\ h^{-1}$ and $K_M = 1 \times 10^{-4}$.

DNA cleavage reactions were also monitored under "true" Michaelis−Menten conditions using a constant complex concentration (60 μM) and varying DNA concentrations (20−160 μM) (Figure 10B), and the

(58) Dhar, S.; Reddy, P. A. N.; Nethaji, M.; Mahadevan, S.; Saha, M. K.; Chakravarty, A. R. *Inorg. Chem.* **2002**, *41*, 3469.

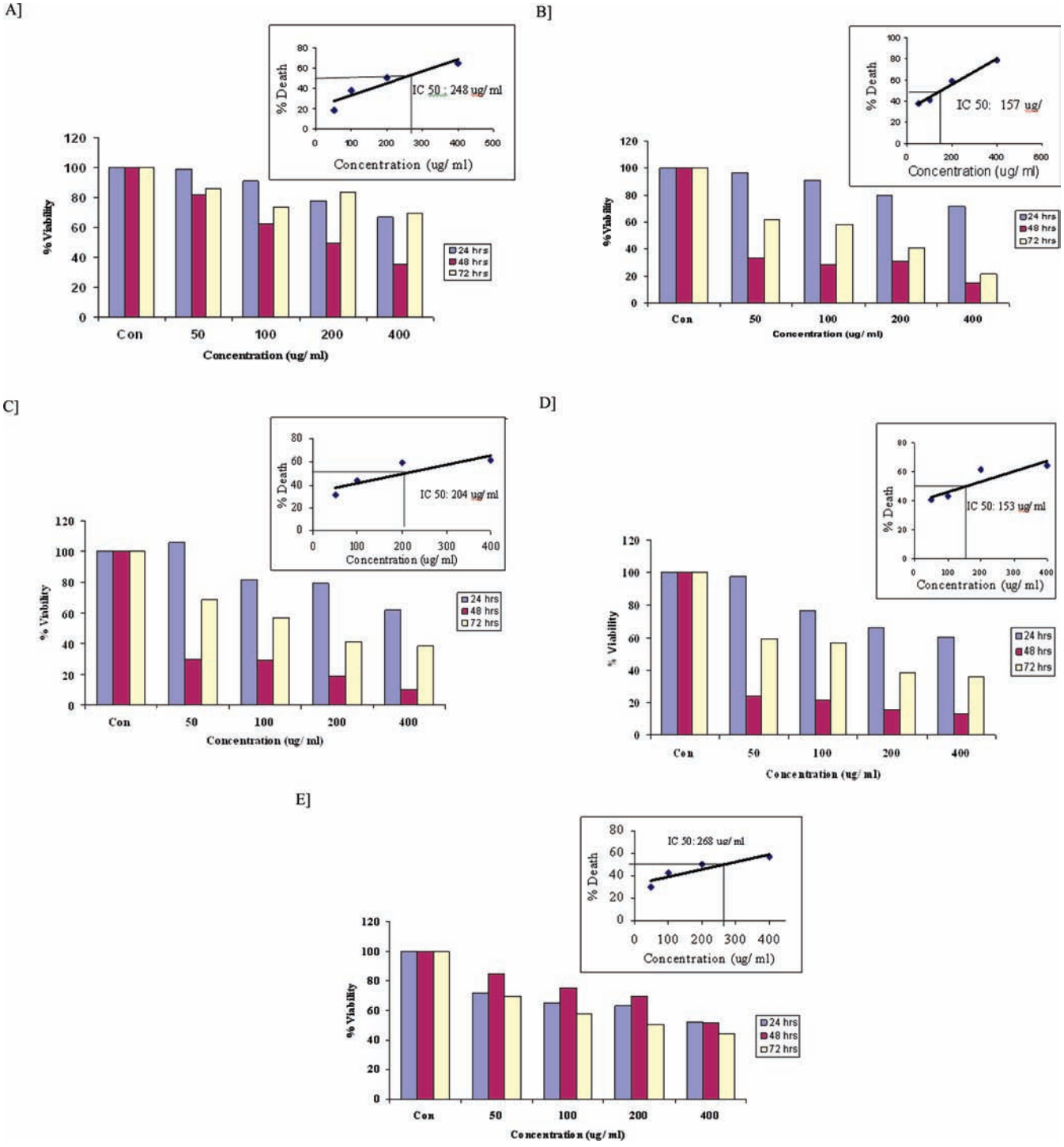

Figure 13. (A) Treatment of HeLa cells with complexes **1**−**5** showed a cytotoxic effect in a concentration-dependent manner. HeLa cells were treated in the absence and presence of complexes **1**−**5**. The cell viability was measured after 24, 48, and 72 h by MTT assay. Each data point represents the mean for three separate experiments.

rates of DNA cleavage were calculated.[57c,49b] Under these conditions, **2** binds to plasmid DNA in an enzyme-like manner with $V_{max}' = 0.0095\ h^{-1}$ and $K_M = 1.4 \times 10^{-4}$.

T4 Ligase Assay. To ascertain the mechanism of DNA cleavage by complexes **1**−**5**, the form II (NC) obtained from the cleavage of SC DNA has been isolated, treated with T4 ligase enzyme, and subjected to electrophoresis.[57c] All complexes are able to ligate DNA fragments. The extent of relegation is ∼30% in complexes **1** and **2**, while in the case of complexes **3** and **4**, it is around 50%, and in complex **5**, a maximum religation of 70% is observed.

Molecular Modeling. To obtain further support for the above DNA binding modes suggested on the basis of the experimental results, the molecular mechanics calculations have been carried out for these copper(II) polypyridyl complexes with the models of right-handed B-DNA of sequence $d(C:G)_{12}$. Considering all possible steric factors, copper(II) complexes **1**−**5** with different

Table 10. Binding Energies (kcal/mol) and Hydrogen-Bond Formation of Copper(II) Polypyridyl Complexes **1**−**5** with Right-Handed B-DNA of Sequence $d(C:G)_{12}$

complexes	energy (kcal mol^{-1})	hydrogen bond	distance (Å)
1	−24 582.968	minor groove	
		O2N (ligand)---N2−H21 (DNA)	2.23
		O2A (ligand)---N2−H21 (DNA))	2.40
2	−24 580.668	minor groove	
		O1−H12 (ligand)---O4′ (DNA)	2.34
3	−20 764.520	partial intercalation	
		no hydrogen bonds	
4	−19 938.652	partial intercalation	
		no hydrogen bonds	
5	−19 635.839	minor groove	1.87
		N5B−H5B (ligand)---O1P (DNA)	

Table 11. IC_{50} and LC_{50} Values for Complexes **1**−**5** Evaluated by MTT Assay and the Brine Shrimp Method

complex	IC_{50} (μg mL^{-1})	LC_{50} (μg mL^{-1})
1	248	> 5.20
2	157	> 3.05
3	204	> 15
4	153	> 15
5	268	> 2.28

orientations in the major/minor grooves of B-DNA were minimized. While carrying out simulation of nucleic acids, it is of utmost importance to calculate the long-range electrostatics accurately. Therefore, the Ewald summation method, which expands the simple sum of Coulombs' law terms into several sums including direct, reciprocal terms, was used. The initial 1000 steps of the steepest-descent minimization were performed to relax the initial strain on the molecule. Further, 1000 steps of conjugate gradient minimization relaxed the molecule completely and decreased the total potential energy. Different modes of binding with different orientations of copper complexes, including groove binding through major/minor grooves, were attempted with the model of right-handed B-DNA of sequence $d(C:G)_{12}$. It is observed that the minimized structure maintains the square-pyramidal form of the complexes and shows hydrogen bonding to the bases and phosphates of DNA in complexes **1**, **2**, and **5** without disrupting the helical structure of B-DNA, while in complexes **3** and **4**, partial intercalation is observed (Figures 12 and S11 in the Supporting Information). The energy calculated also indicates a minor groove affinity for complexes **1**, **2**, and **5**, which corroborates our experimental observation using distamycin assay.

Study of Toxicity by MTT Assay. MTT assay was performed to check the antineoplastic effect of complexes **1**−**5**. Complexes showed significant in vitro antineoplastic activity after 24, 48, and 72 h, and their effects on the cellular viability were evaluated. A decrease in the percent of cell viability was observed with all of the complexes, but a maximum and significant decrease was observed with complex **4**. The 95% decrease in cell growth was observed with 200−400 μg mL^{-1} of complex **4** after 48 h, which decreased to 60% after 72 h. Complex **3** (200−400 μg mL^{-1}) also showed significant decreases of 90 and 80% after 48 h, which increased after 72 h. Complexes **1** and **2** showed no significant cell growth reduction in 24 h, but the cell viability reduced after 48 h with 60 and 80%. Complex **5** shows different cell death patterns in which there is a time course percent of cell viability observed after 24, 48, and 72 h of incubation. The maximum cell death was observed with 200−400 μg mL^{-1} of complex **5**. The cytotoxicities of the complexes correlate well with the planarity of the ligand as seen by the IC_{50} value in Table 11.

Study of Toxicity by the Brine Shrimp Method. The toxicity of the copper complexes **1**−**5** was also evaluated by the brine shrimp method, which is a preliminary test for cytotoxicity. In complex **1**, 80% dead larvae are observed at 480 μg, while in complexes **2** and **5**, 100% dead larvae are observed at 240 μg and complexes **3** and **4** show 100% dead larvae after treatment with a 120 μg concentration dose. LC_{50} values are less than 15 μg in all complexes (Table 11).

Conclusions

Mixed-ligand copper(II) complexes of the maltolate ligand with a series of diimine ligands have been synthesized and characterized spectroscopically. X-ray crystal structures of complexes exhibit copper(II) located in square-pyramidal geometries. The coordinated bpy, phen, phendione, and bpg coligands of the mixed-ligand copper(II) complexes involve either partial intercalation or groove binding into DNA base pairs, while dppz intercalates in the major groove but the strength of intercalation is less as compared to classical intercalators.

All complexes hydrolyze NPP with moderate rate constants. All complexes cleave SC plasmid DNA by a hydrolytic cleavage mechanism in the absence of any external added reagent. Molecular modeling studies show that the phendione and dppz complexes intercalate partially while the others bind electrostatically in the minor groove with hydrogen-bonding interactions with phosphates. The complexes are cytotoxic to HeLa cell lines as well as brine shrimp larvae with low IC_{50} and LC_{50} values, respectively.

Acknowledgment. A.B. acknowledges the Department of Science and Technology (DST), New Delhi, India, for financial support in the form of a predoctoral fellowship under "New Initiatives in Bioinorganic Chemistry" (SR/S1/PRD-06//2006). A.K. acknowledges funding from DST, New Delhi (SR/S5/BC-25/2006), and UGC, New Delhi (No. 32-198/2006(SR), and University of Pune for partial funding. The authors thank Dr. S. Sarkar, IIT Kanpur, for single-crystal X-ray data of complex **2**. The authors thank Dr. Anupa A. Kumbhar from the Department of Chemistry for discussion and Rashmi, Meghana,

and Sharvari from the Institute of Bioinformatics and Biotechnology, Pune, India, for their help.

Supporting Information Available: Packing diagram of complexes **1**, **2**, and **5** (Figures S1−S3), UV−vis spectra of complexes **1**−**5** (Figure S4), ESR spectra of complexes **1**−**5** (Figure S5), single-crystal ESR spectra of complexes **1**, **2**, and **5** (Figure S6), angular variations of *g* values in a random plane (Table S1), competitive binding fluorescence measurements of EBR (Figure S7), DNA cleavage in the presence of radical scavengers (Figure S8), distamycin assay (Figure S9), molecular modeling (Figure S10), and MTT assay for complexes **1**−**5** against a HeLa cell line (Figure S11). This material is available free of charge via the Internet at http://pubs.acs.org. Crystallographic data for complexes **1**, **2**, and **5** have been deposited at the Cambridge Crystallographic Data Center as CCDC numbers 673676, 673677, and 673678. Any inquiries relating to the data can be e-mailed to deposit@ccdc.cam.ac.uk.